Electronic Supplementary Material (ESI) for Molecular BioSystems

Supporting Information

Identification of Polyoxometalates as Inhibitors of Basic Fibroblast Growth Factor

Table of contents

1. Experimental section
2. **Figure S1.** FTIR spectra of POMs.
3. **Figure S2.** Stability of POMs characterized by UV/vis spectroscopy.
4. **Figure S3.** Fluorescence quenching of bFGF by POMs.
5. **Figure S4.** Temperature-dependent CD spectra.
6. **Figure S5.** Fluorescence spectra of bFGF in the absence and presence of urea.
7. **Figure S6.** Unfolding kinetics of bFGF.
8. **Figure S7.** Time-dependent SDS-PAGE of bFGF digested by trypsin.
9. **Figure S8.** The crystal structure of the 154-amino-acid form of human basic fibroblast growth factor.
10. **Figure S9.** SDS-PAGE of HSA digested by trypsin in the absence and presence of POMs.
11. **Figure S10.** Non-reducing PAGE experiments of bFGF in the absence and presence of POMs.
12. **Figure S11.** Far-UV CD spectra of bFGF in the presence of POM or heparin in 40% TFE.
13. **Figure S12.** The replacement of POM α-$Na_9H[SiW_9O_{34}]$ on bFGF by heparin monitored by RLS.
14. **Figure S13.** The crystal structure of the 154-amino-acid form of human basic fibroblast growth

factor. The amino acids labeled in the figure are putative contributors to heparin binding.

15. **Figure S14.** The interaction between bFGF and other two Wells-Dawson structure POMs.

16. **Figure S15.** Thermal denaturation and trypsin digestion assays of POMs containing Mo.

17. **Figure S16.** MTT assay for inhibition of POMs on the HUVEC proliferation induced by bFGF.

18. **Figure S17.** Comparison of the bFGF inhibition by POMs for HUVEC.

19. **Figure S18.** Inhibition of DNA synthesis by POMs.

Experimental section

Materials, Methods and Instrumentation:

Human bFGF was provided by Bio-Engineering Institute of Jinan University. bFGF samples of various concentrations were prepared in PBS solution (20 mM sodium phosphate, 150 mM NaCl, pH 7.4). Protein concentration was determined spectrophotometrically using an extinction coefficient of E (0.1%, 1 cm) = 0.964 at 280 nm. The others are of analytical or biochemical grade reagents and used as supplied.

The polyoxometalates used were synthesized according to procedures established by Key Laboratory of Polyoxometalate Science of the Ministry of Education (Northeast Normal University) and published elsewhere ($Na_5IMo_6O_{24}$, $K_7[PTi_2W_{10}O_{40}]$ and $H_3PMo_{12}O_{40}$)[1-3]. The purity of all tested compounds was determined by ICP atomic emission spectrometer and Fourier transform infrared (FTIR) spectrometer, and was greater than 95%. FTIR analyses were carried out on a Bruker Vertex 70 FT-IR Spectrometer.

Synthesis of α-$Na_9H[SiW_9O_{34}]$: HCl (6 M, 130 mL) was added into an aqueous solution (200 mL) containing Na_2WO_4•$2H_2O$ (182 g) and Na_2SiO_3•$9H_2O$ (12 g) under vigorous stirring. Then, the obtained solution was boiled for 1 h and condensed into 300 mL. After filtration, Na_2CO_3 (50 g) dissolved in water (150 mL) was added to the filtrate. After stirring, the precipitate was collected by filtration and dried.

Elemental analysis:

(1) $Na_5IMo_6O_{24}$ (Calculated: Na, 9.57%; Mo, 47.91%; I, 10.56%, O, 31.96%. Found: Na, 9.64%; Mo, 47.82%; I, 10.48%; O, 32.06%)

(2) $La_2K[PTi_2W_{10}O_{40}]\cdot 8H_2O$ (Calculated: P, 1.01%; W, 59.95%; K, 1.27%; Ti, 3.12%; La, 9.06%; O, 25.05%; H, 0.53%. Found: P, 1.06%; W, 59.99%; K, 1.32%; Ti, 3.20%; La, 9.05%; O, 24.90%; H, 0.49%)

(3) $La_2K_4[GeTi_3W_9O_{40}]$ (Calculated: Ge, 2.47%; W, 56.18%; K, 5.31%; Ti, 4.88%; La, 9.43%; O, 21.73%. Found; Ge, 2.54%; W, 56.17%; K, 5.36%; Ti, 4.86%; La, 9.47%; O, 21.61%)

(4) $K_7[PTi_2W_{10}O_{40}]\cdot 6H_2O$ (Calculated: P, 1.04%; W, 61.55%; K, 9.16%; Ti, 3.21%; O, 24.64%; H, 0.40%. Found: P, 1.11%; W, 61.48%; K, 9.23%; Ti, 3.24%; O, 24.59%; H, 0.35%)

(5) α-$Na_9H[SiW_9O_{34}]\cdot 16H_2O$ (Calculated: Si, 1.03%; W, 60.76%; Na, 7.60%; O, 29.38%; H,1.22%. Found; Si, 1.02%; W, 60.64%; Na, 7.69% O, 29.45%; H,1.20%)

(6) $K_8[\beta\text{-}SiW_{11}O_{39}]\cdot 14H_2O$ (Calculated: Si, 0.87%; W, 62.43%; K, 9.66%; O, 26.18%; H, 0.87%. Found: Si, 0.81%; W, 62.78%; K, 9.64%; O, 25.98%; H, 0.79%)

(7) $(NH_4)_6[P_2W_{18}O_{62}]\cdot H_2O$ (Calculated: P, 1.38%; W, 73.71%; N, 1.87%; O, 22.45%; H, 0.58%. Found: P, 1.29%; W, 74.11%; N, 1.83%; O, 22.25%; H, 0.53%)

(8) $H_3PMo_{12}O_{40}$ (Calculated: P, 1.70%; Mo, 63.08%; O, 35.06%; H, 0.17%. Found: P, 1.77%; Mo, 63.17%; O, 34.9%; H, 0.16%)

Reference

[1] M. Filowitz, R. K. C. Ho, W. G. Klemperer, W. Shum, ^{17}O Nuclear Magnetic-Resonance Spectroscopy of Polyoxometalates .1. Sensitivity and Resolution, Inorg. Chem. 18 (1979) 93-103.

[2] P. J. Domaille, W. H. Knoth, $Ti_2W_{10}PO_{40}^{7-}$ and $[CpFe(CO)_2Sn]_2W_{10}PO_{38}^{5-}$. Preparation, properties, and structure determination by tungsten-183 NMR, Inorg. Chem. 22 (1983) 818-822.

[3] H. Wu, Contribution to the chemistry of phosphomolybdic acids, phosphotungstic acids, and allied substances, J Biol. Chem. 43 (1920) 189-220.

Methods

Resonance light scattering (RLS)

The RLS spectrum was recorded with a JASCO FP6500 Spectrophotometer by simultaneously

scanning the excitation and emission monochromators of the spectrofluorometer from 220 to 750 nm with $\Delta\lambda = 0$ nm.

Thermal denaturation experiments using circular dichroism

Thermal curve of protein were determined by using a JASCO 810 Spectrophotometer. Thermal unfolding experiments monitored the change in ellipticity as a function of temperature and were performed under computer control by increasing the temperature of the water bath at the speed of 1.0 ℃/min. The scan of buffer alone recorded at room temperature was subtracted.

Non-reducing PAGE

Samples were solubilized in PBS without reducing agent and without boiling unless otherwise indicated. After electrophoresis, protein was visualized by staining with Coomassie Brilliant Blue.

Urea-induced unfolding experiments

The rate and extent of urea-induced unfolding of the protein in the presence and absence of POMs were monitored by fluorescence spectroscopy. Unfolding kinetics studies were performed by mixing bFGF in PBS containing the desired amounts of POMs with urea in PBS. After an initial mixing period (ca. 10 s), the fluorescence spectra were recorded at 2-second intervals by monitoring the emission at 350 nm.

TFE-induced formation of α-helix

2, 2, 2-Trifluorethanol (TFE) has been routinely used as a structure-inducing cosolvent. TFE can induce helical conformation in a protein which has no sequence propensity. The helical structures induced by TFE were monitored by far-UV Circular Dichroism with a JASCO 810 spectrophotometer. The protein concentration was 4 μM, in 0.1 cm path-length cells, in an average of 4 scans between 195 and 260 nm, with a 1.0 nm bandwidth, a scanning rate of 10nm/min.

Direct thiol titration studies

35 μL of DTNB reagent solution (4 mg/mL) was added to tubes containing bFGF (5 μM, 500 μL, 20 mM Tris, 150 mM KCl, pH 8) and bFGF-POMs complexes, respectively. Mix and incubate at room

temperature for 30 minutes. With a spectrophotometer set to 412 nm, zero the instrument on the blank and then measure absorbance of each sample. Calculate the amount of free SH in the samples.

MALDI-TOF MS process

Samples were deposited on the MALDI target using dried droplet method. MALDI-TOF MS experiment were performed in positive ion mode on an AutoflexⅢTOF/TOF Analyzer (Bruker Daltonics Inc, Germany) with the Nd-YAG laser operated at 355 nm with 0 ns duration pulses, a repletion rate of 200 Hz and an acceleration voltage of 19 kV. MS spectra were acquired as an average of 100 laser shots for two times.

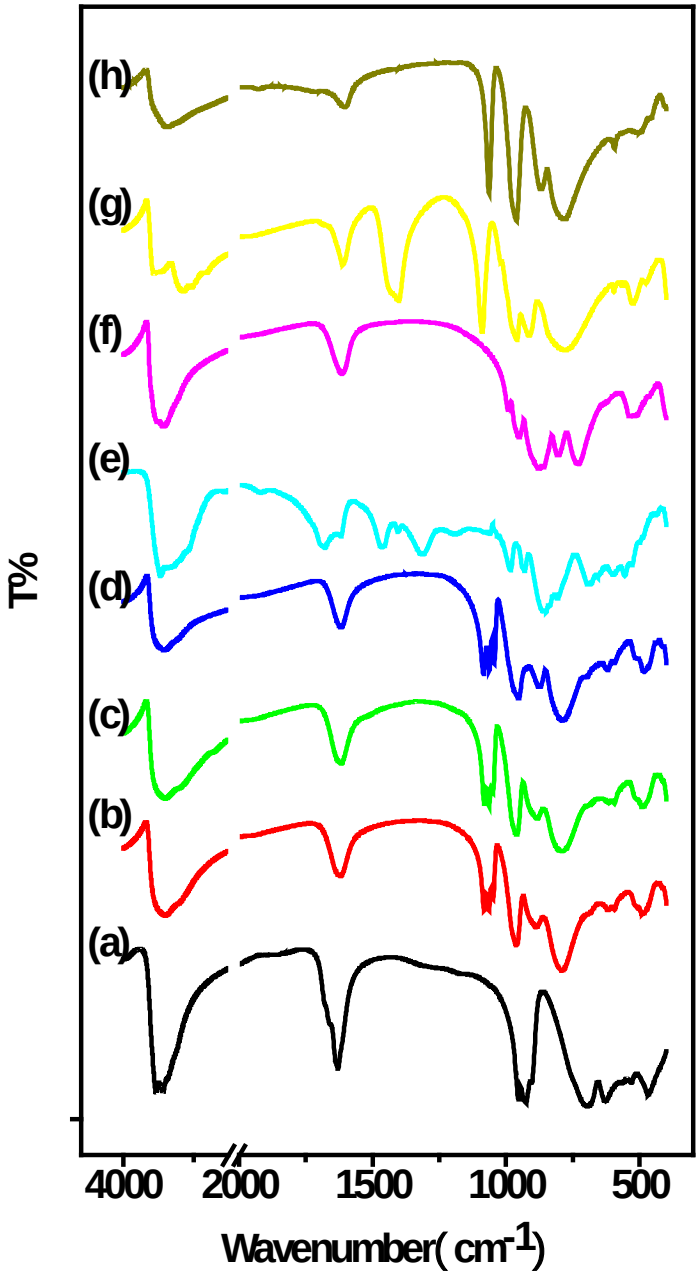

Figure S1. FTIR spectra of POMs. (a) $Na_5IMo_6O_{24}$; (b) $La_2K[PTi_2W_{10}O_{40}]$; (c) $La_2K_4[GeTi_3W_9O_{40}]$; (d) $K_7[PTi_2W_{10}O_{40}]$; (e) α-$Na_9H[SiW_9O_{34}]$; (f) $K_8[\beta\text{-}SiW_{11}O_{39}]$; (g) $(NH_4)_6[P_2W_{18}O_{62}]$; (h) $H_3PMo_{12}O_{40}$.

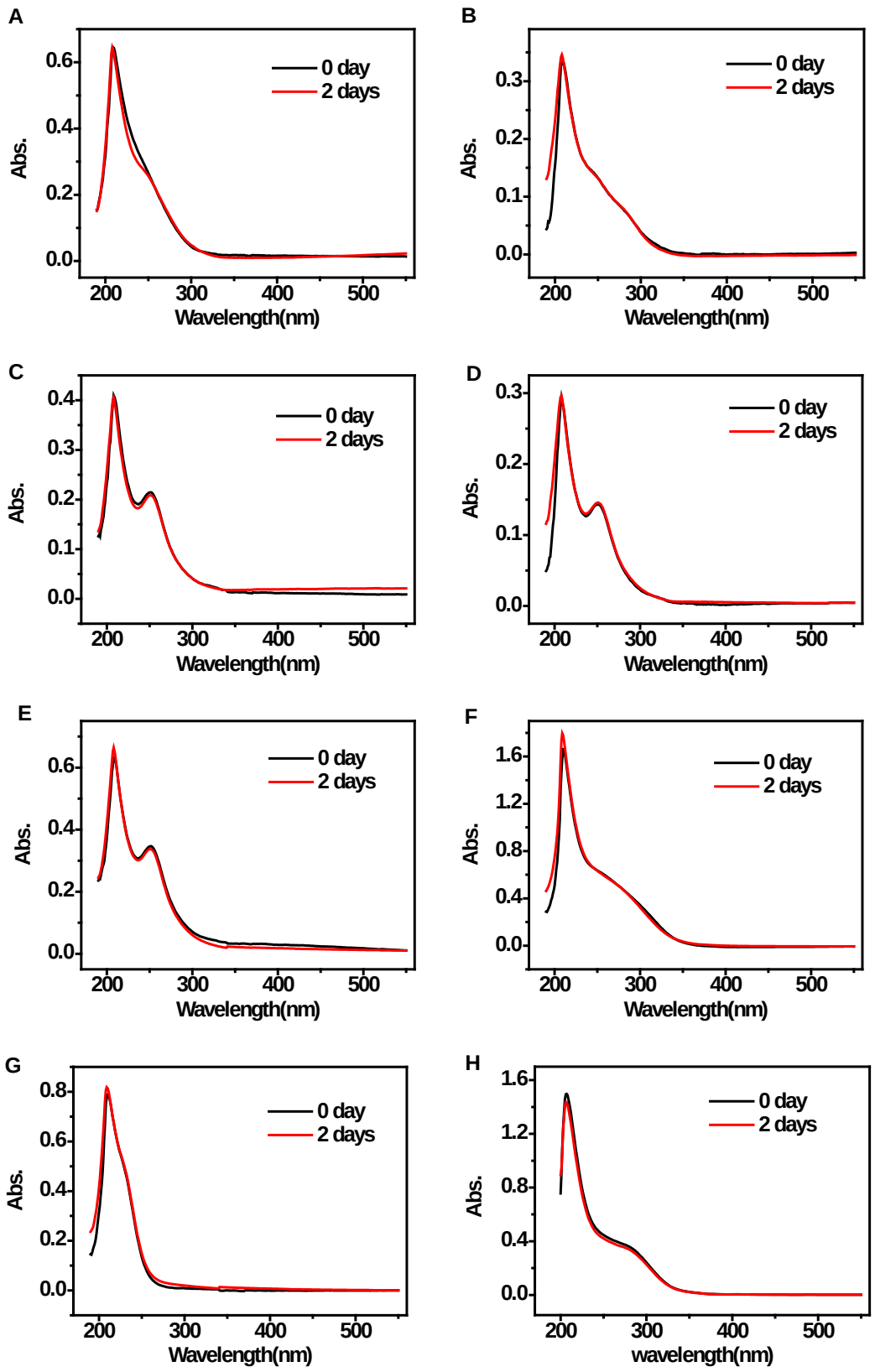
A
B
C
D
E
F
G
H
0 day
2 days
Abs.
Wavelength(nm)
wavelength(nm)

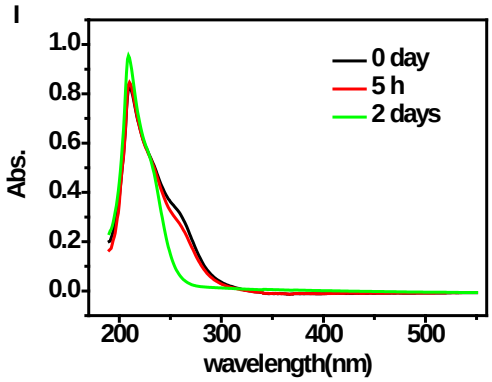

Figure S2. Stability of POMs characterized by UV/vis spectroscopy. Experiments were performed in PBS buffer (20 mM sodium phosphate, 150 mM NaCl, pH 7.4). (A) α-$Na_9H[SiW_9O_{34}]$; (B) $K_8[\beta\text{-}SiW_{11}O_{39}]$; (C) $La_2K[PTi_2W_{10}O_{40}]$; (D) $K_7[PTi_2W_{10}O_{40}]$; (E) $La_2K_4[GeTi_3W_9O_{40}]$; (F) $(NH_4)_6[P_2W_{18}O_{62}]$; (G) $Na_5IMo_6O_{24}$; (H) $K_8[P_2CoW_{17}O_{61}]$; (I) $H_3PMo_{12}O_{40}$. $H_3PMo_{12}O_{40}$ exhibited limited stability, but the assay conditions (fresh preparation of test solution, fast assay within a few minutes) were such that degradation should be negligible.

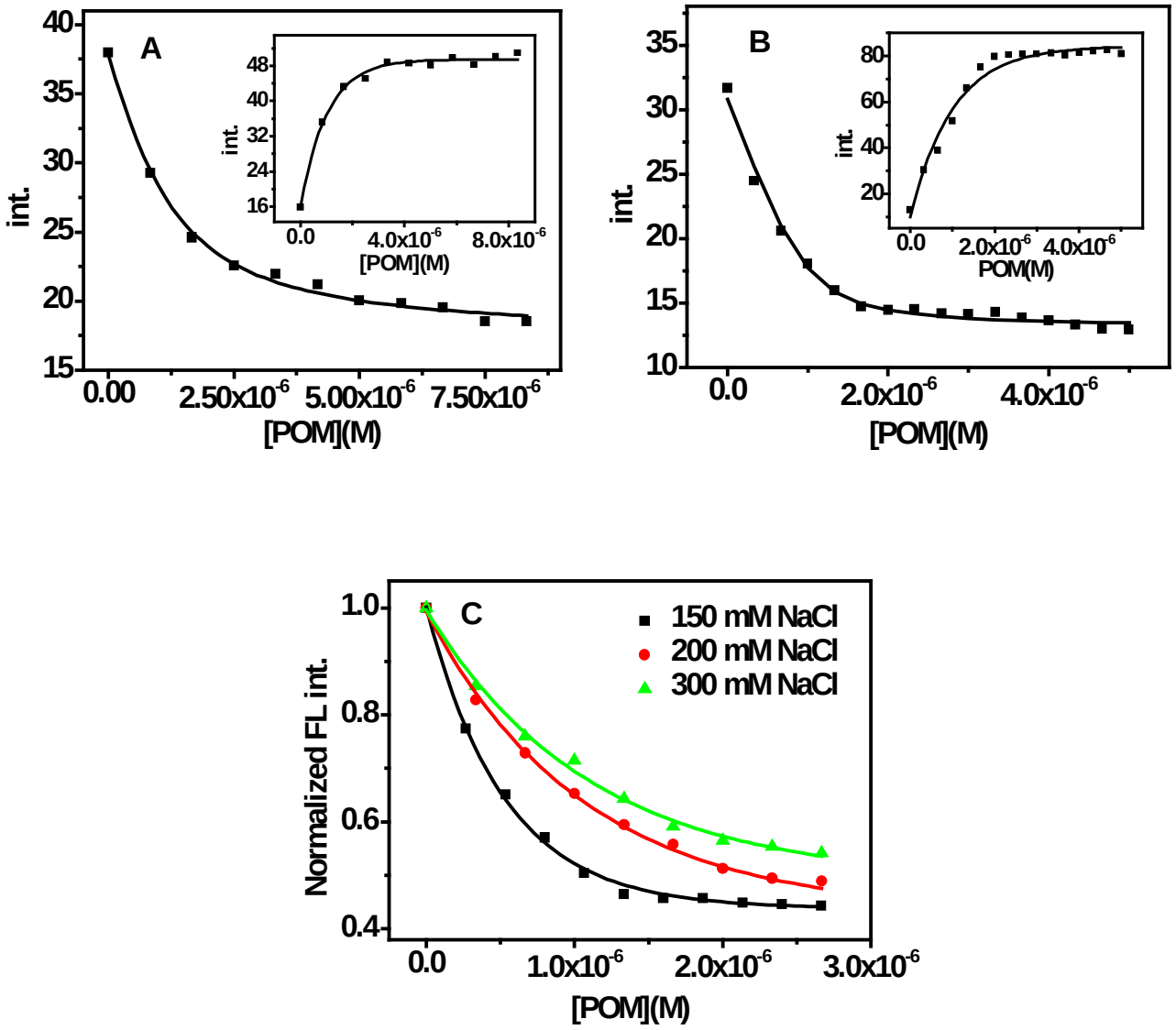

Figure S3. Fluorescence quenching of bFGF by POMs. The fluorescence emission of bFGF (2 μM), in the presence of variable concentration of (A) $K_8[\beta\text{-}SiW_{11}O_{39}]$ or (B) $(NH_4)_6[P_2W_{18}O_{62}]$, was followed at λex = 280 nm, λem = 305 nm. The inset showed the change of RLS spectrum of bFGF-POMs complex with increase of concentration of POMs. (C) The fluorescence quenching of bFGF by POM $La_2K[PTi_2W_{10}O_{40}]$ in the presence of variable concentrations of NaCl.

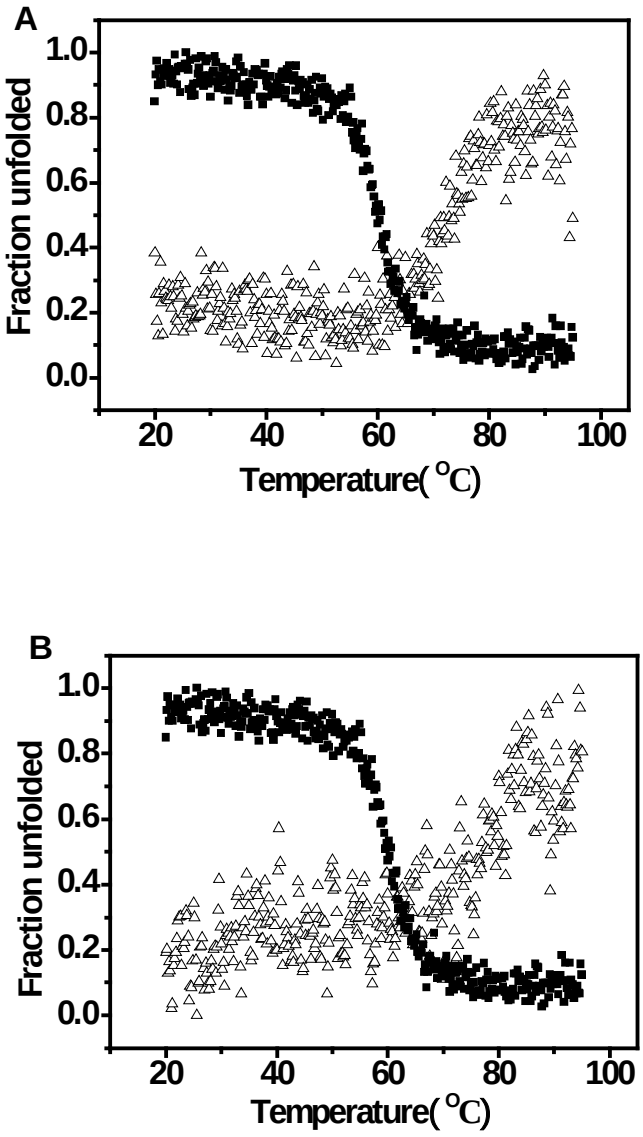

Figure S4. Temperature-dependent CD spectra of bFGF alone (■) monitored at 229 nm and bFGF in the presence of POMs (△) monitored at 204 nm. [bFGF] = 5 μM, and the ratio of bFGF to (A) $K_8[\beta\text{-}SiW_{11}O_{39}]$ or (B) $(NH_4)_6[P_2W_{18}O_{62}]$ was 1:4.

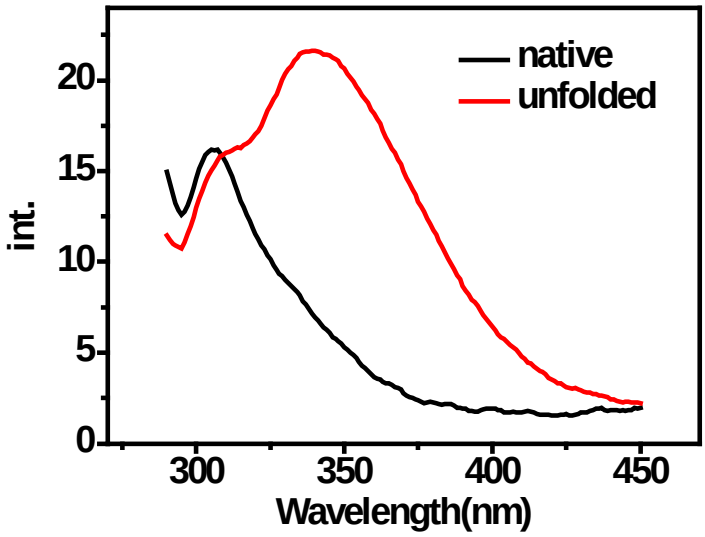

Figure S5. Fluorescence spectra of bFGF in the absence and presence of urea, λex = 280 nm.

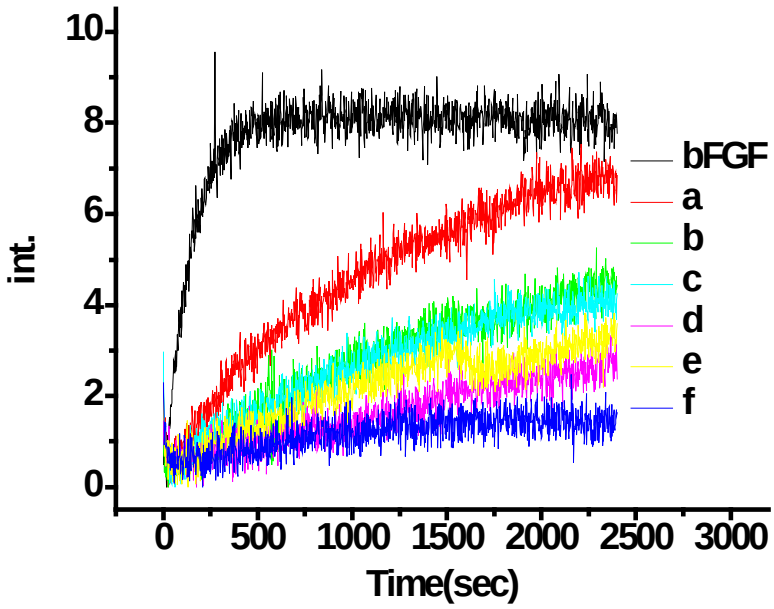

Figure S6. Unfolding kinetics of bFGF in 4 M urea in the absence and presence of POMs (a) $(NH_4)_6P_2W_{18}O_{62}$, (b) $K_8[\beta\text{-}SiW_{11}O_{39}]$, (c) $La_2K[PTi_2W_{10}O_{40}]$, (d) $La_2K_4[GeTi_3W_9O_{40}]$, (e) $K_7[PTi_2W_{10}O_{40}]$, and (f) $\alpha\text{-}Na_9H[SiW_9O_{34}]$, monitored by fluorescence spectroscopy. λex = 280 nm, λem = 350 nm.

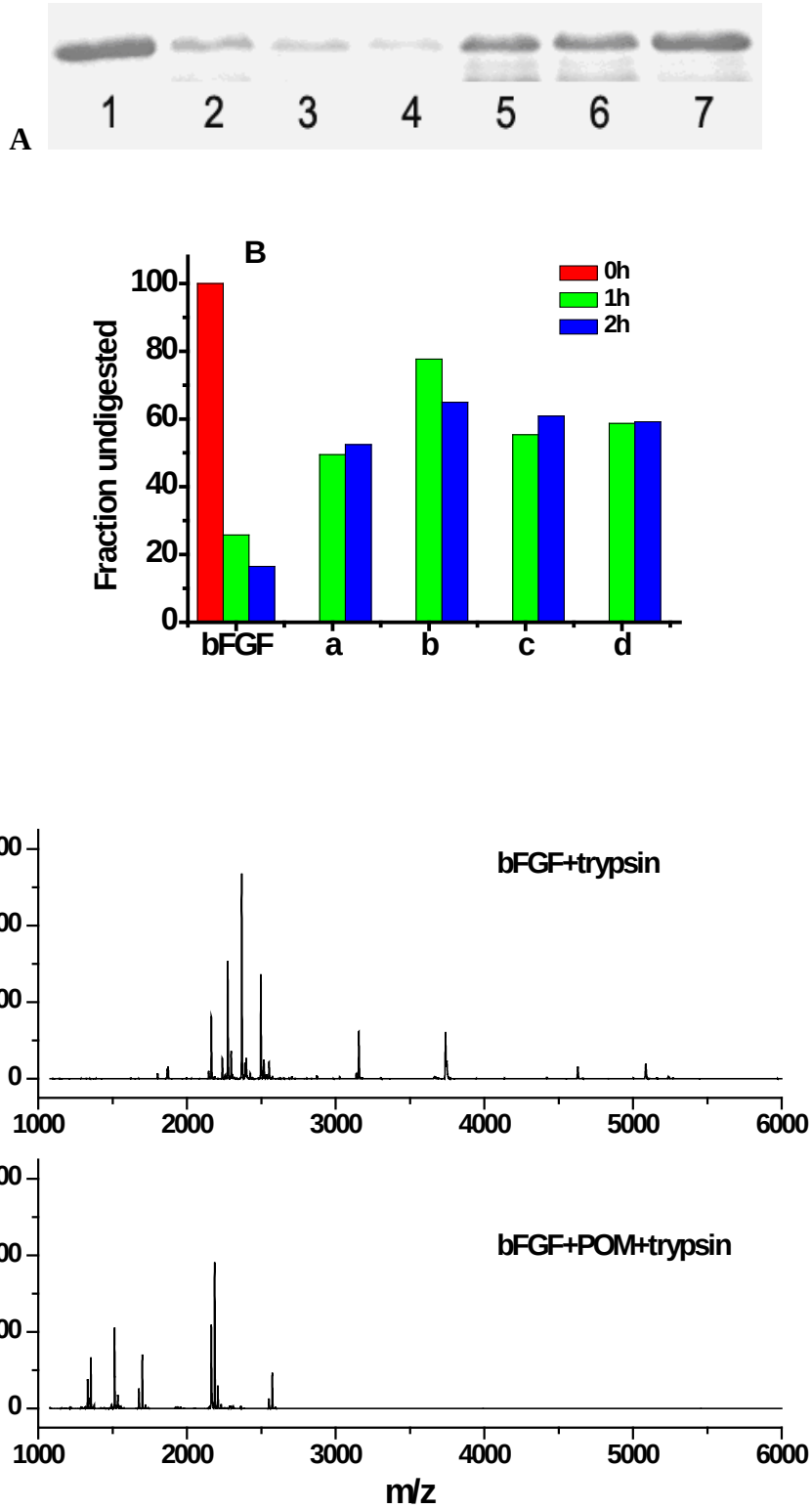

Figure S7. (A) Time-dependent SDS-PAGE of bFGF digested by trypsin in the absence and presence of POMs. Lane1. bFGF; Lane2-4. the digestion products of bFGF within 1, 2, and 4 h; Lane5-7. the

digestion products of bFGF in the presence of POM α-$Na_9H[SiW_9O_{34}]$ within 1, 2, and 4 h. (B) Semi-quantification of the trypsin cleavage products of bFGF in the presence of POMs (a) α-$Na_9H[SiW_9O_{34}]$, (b) $K_8[\beta\text{-}SiW_{11}O_{39}]$, (c) $La_2K[PTi_2W_{10}O_{40}]$, and (d) $K_7[PTi_2W_{10}O_{40}]$. (C) MALDI-TOF mass spectra of bFGF digested by trypsin in the absence and presence of POM $(NH_4)_6P_2W_{18}O_{62}$. Upon the addition of POM, the basic cluster including Arg and Lys residues on the surface of bFGF might be masked by POM. Trypsin could not cleave this site.

Table 1. The search results of bFGF digested by trypsin in the absence and presence of POM $(NH_4)_6P_2W_{18}O_{62}$.

bFGF+trypsin		
Start-End	m/z	Sequence
120-134	1865.1552	YTSWYVALKRTGQYK
62-81	2169.1687	LQLQAEERGVVSIKGVCANR
36-55	2270.5747	NGGFFLRIHPDGRVDGVREK
87-106	2366.6933	EDGRLLASKCVTDECFFFER
1-27	2496.7995	MAAGSITTLPALPEDGGSGAFPPGHFK
130-155	2710.2312	TGQYKLGSKTGPGQKAILFLPMSAKS
1-13	2879.2188	MAAGSITTLPALPEDGGSGAFPPGHFKDPK
91-116	3164.5647	LLASKCVTDECFFFERLESNNYNTYR
54-86	3729.3859	EKSDPHIKLQLQAEERGVVSIKGVCANRYLAMK
76-118	5088.7693	GVCANRYLAMKEDGRLLASKCVTDECFFFERLESNNYNTYRSR

bFGF+POM+trypsin		
Start-End	m/z	Sequence
107-118	1517.6076	LESNNYNTYRSR
130-144	1550.7656	TGQYKLGSKTGPGQK
76-90	1699.9601	GVCANRYLAMKEDGR
117-134	2236.5977	SRKYTSWYVALKRTGQYK
70-90	2283.6935	GVVSIKGVCANRYLAMKEDGR
87-106	2366.6933	EDGRLLASKCVTDECFFFER

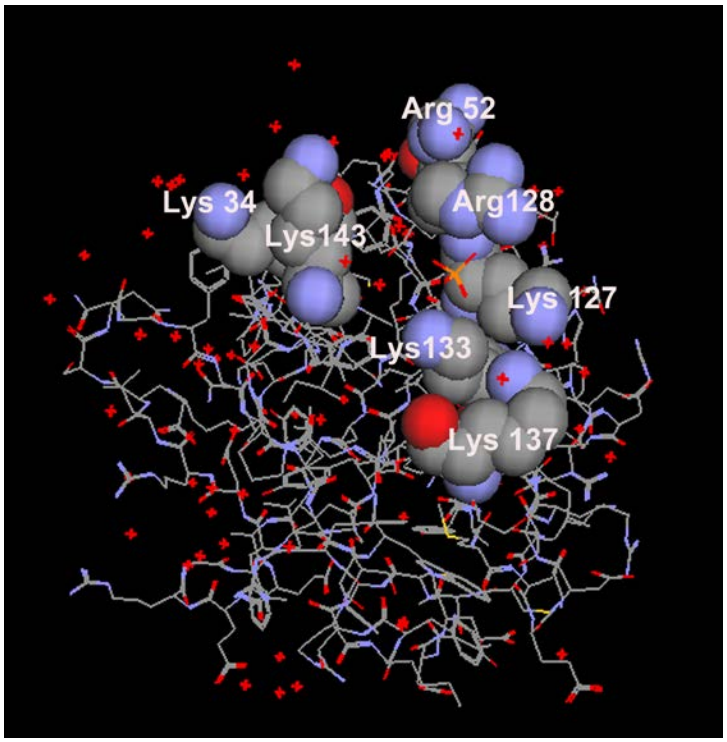

Figure S8. The crystal structure of the 154-amino-acid form of human basic fibroblast growth factor (hbFGF154), taken from the PDB (Acta Crystallogr. D Biol. Crystallogr. 1997, 53, 60-168). Crystals were obtained from recombinant hbFGF154 expressed in E. coli. On the surface of bFGF there is a cluster of basic residues including Lys 34, 127, 133, 137, 143, and Arg 52, 128, which are labeled in the figure.

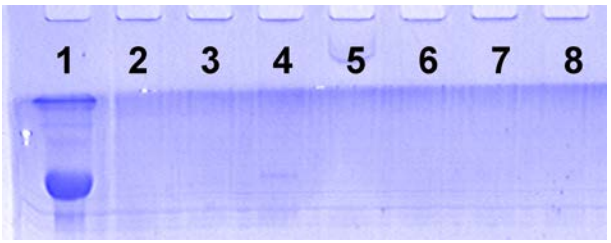

Figure S9. SDS-PAGE of HSA digested by trypsin in the absence and presence of POMs. Lane1. HSA; Lane2. the digested product of HSA; Lane3-8. the digested product of HSA in the presence of α-$Na_9H[SiW_9O_{34}]$, $K_8[\beta\text{-}SiW_{11}O_{39}]$, $(NH_4)_6[P_2W_{18}O_{62}]$, $La_2K[PTi_2W_{10}O_{40}]$, $La_2K_4[GeTi_3W_9O_{40}]$, and $K_7[PTi_2W_{10}O_{40}]$. The ratio of HSA to POMs was 1:1.

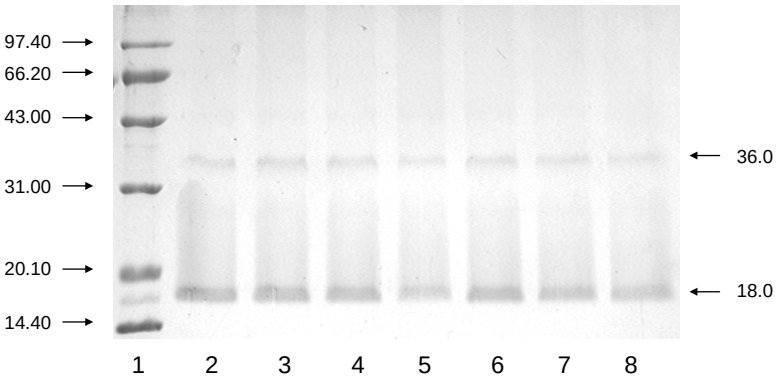

Figure S10. Non-reducing PAGE experiments of bFGF in the absence and presence of POMs. Lane1. DNA marker; Lane2. bFGF; Lane3-8. bFGF in the presence of α-$Na_9H[SiW_9O_{34}]$, $K_8[\beta\text{-}SiW_{11}O_{39}]$, $(NH_4)_6[P_2W_{18}O_{62}]$, $La_2K[PTi_2W_{10}O_{40}]$, $La_2K_4[GeTi_3W_9O_{40}]$, and $K_7[PTi_2W_{10}O_{40}]$. The molar ratio of bFGF to POMs was 1:1.

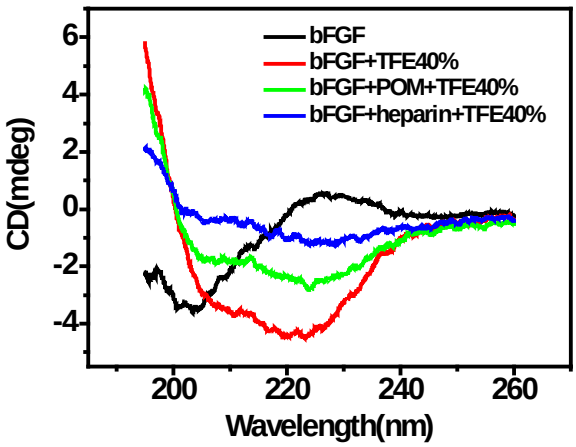

Figure S11. Far-UV CD spectra of bFGF in the presence of POM or heparin in 40% TFE. [bFGF] = 4 μM, and the ratio of bFGF to $K_8[\beta\text{-}SiW_{11}O_{39}]$ was 1:1.

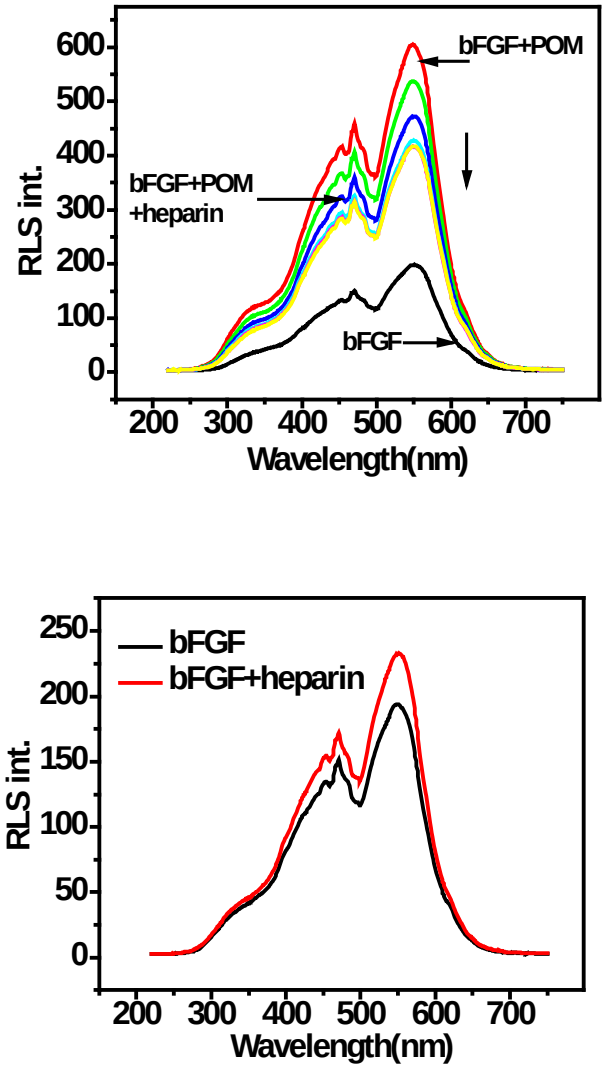

Figure S12. The replacement of POM α-$Na_9H[SiW_9O_{34}]$ on bFGF by heparin monitored by RLS. The ratio of bFGF to POMs was 1:1.

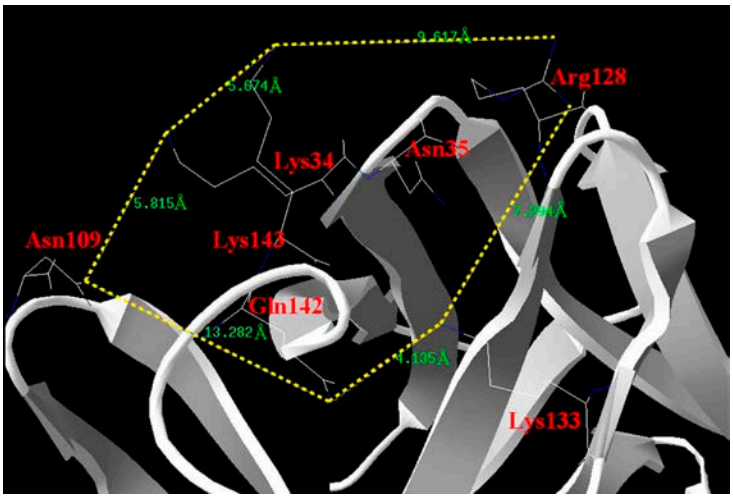

Figure S13. The crystal structure of the 154-amino-acid form of human basic fibroblast growth factor (hbFGF154), taken from the PDB (Acta Crystallogr. D Biol. Crystallogr. 1997, 53, 60-168). The amino acids labeled in the figure are putative contributors to heparin binding.

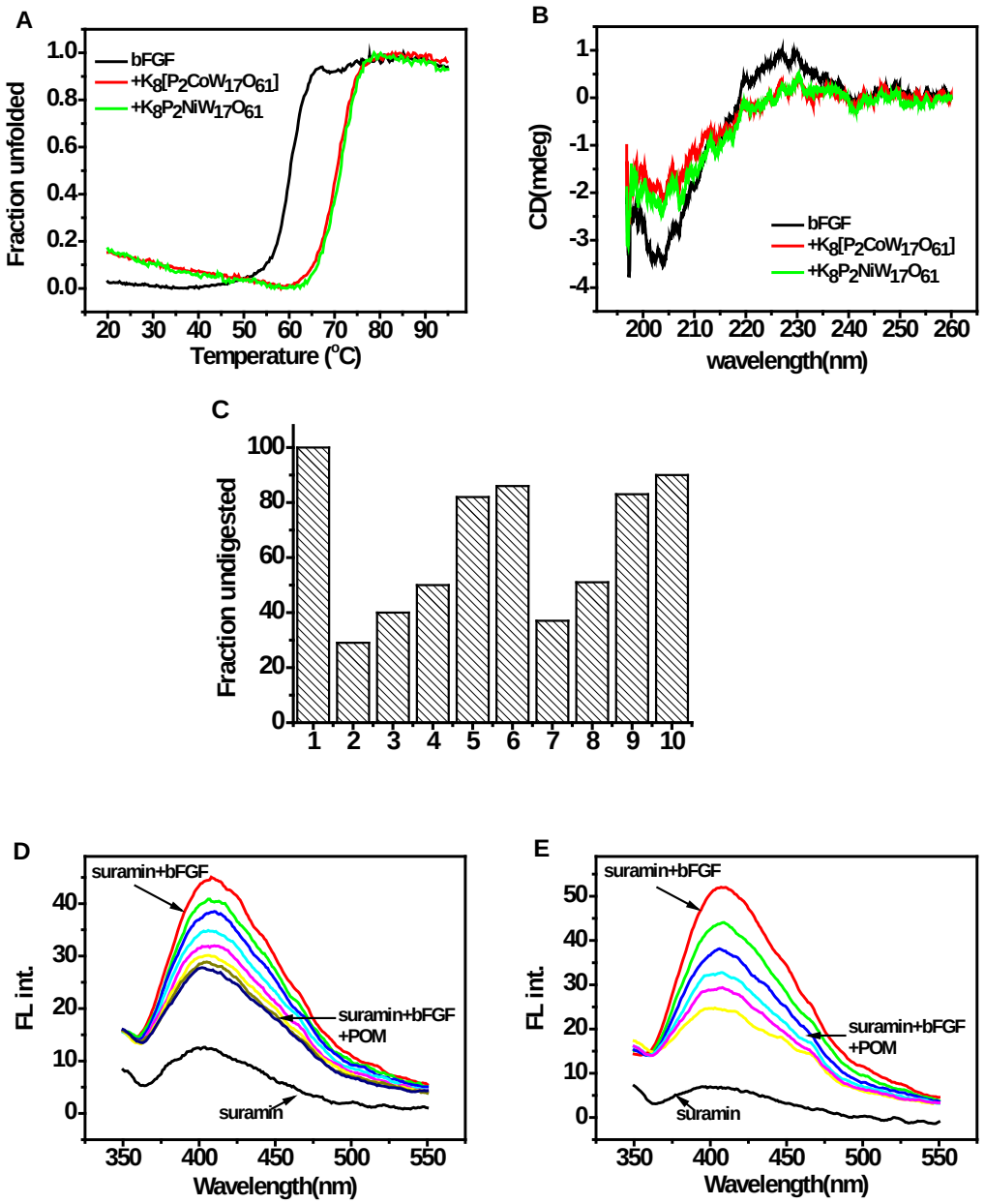

Figure S14. The interaction between bFGF and other two Wells-Dawson structure POMs. (A) UV-melting curves of bFGF with POMs. (B) CD spectra of bFGF in the presence of POMs. (C) Trypsin digestion of bFGF. 1. bFGF; 2. bFGF+trypsin; 3-6. bFGF+ $K_8[P_2CoW_{17}O_{61}]$+trypsin; 7-10. bFGF+ $K_8P_2NiW_{17}O_{61}$+trypsin. (D) Effect of $K_8[P_2CoW_{17}O_{61}]$ on the fluorescence of suramin-bFGF complex. (E) Effect of $K_8P_2NiW_{17}O_{61}$ on the fluorescence of suramin-bFGF complex.

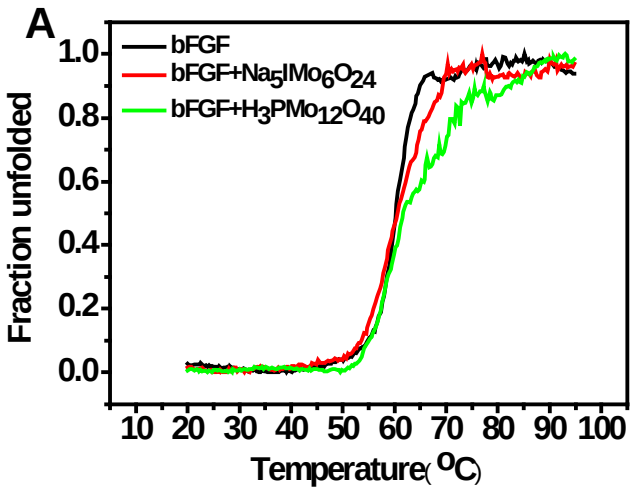

B

Figure S15. (A) Effect of Anderson structure $Na_5IMo_6O_{24}$ and Keggin structure $H_3PMo_{12}O_{40}$ on the thermal stability of bFGF. (B) Trypsin digestion experiment of bFGF in the absence and presence of POMs. Lane 1. bFGF; Lanes 2. the tryptic digestion product of bFGF alone; Lanes 3-4. the digestion products of bFGF in the presence of $Na_5IMo_6O_{24}$ and $H_3PMo_{12}O_{40}$, respectively.

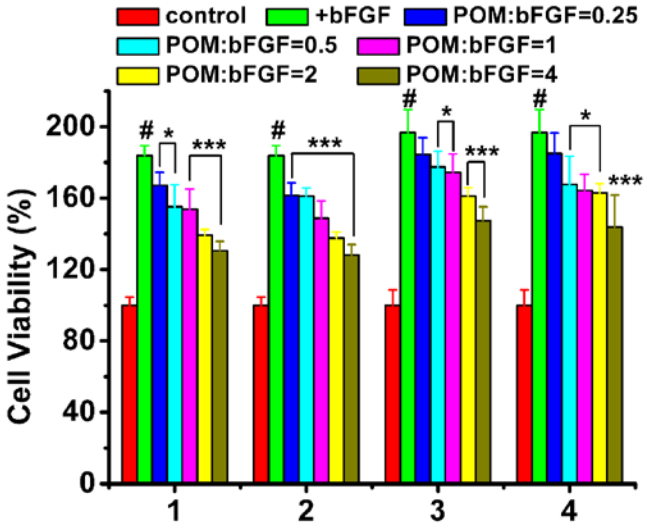

Figure S16. MTT assay for inhibition of POMs on the HUVEC proliferation induced by bFGF. (1) α-$Na_9H[SiW_9O_{34}]$, (2) $K_8[\beta\text{-}SiW_{11}O_{39}]$, (3) $La_2K_4[GeTi_3W_9O_{40}]$, (4) $K_7[PTi_2W_{10}O_{40}$. Results are expressed as percentage of the control, and the data are expressed as the mean ± SD values (n = 5). Statistic results of ANOVA: #, $p<0.001$ vs. the control group; *, $p<0.05$, and ***, $p<0.001$ vs. the bFGF stimulated group.

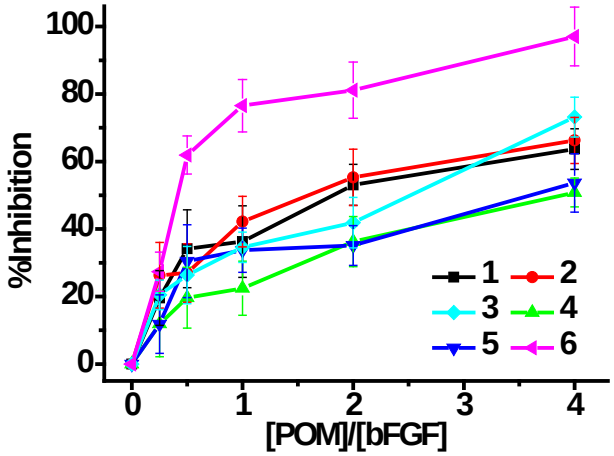

Figure S17. Comparison of the bFGF inhibition by POMs (1) α-$Na_9H[SiW_9O_{34}]$, (2) $K_8[\beta\text{-}SiW_{11}O_{39}]$, (3) $La_2K[PTi_2W_{10}O_{40}]$, (4) $K_7[PTi_2W_{10}O_{40}]$, (5) $La_2K_4[GeTi_3W_9O_{40}]$, and (6) $(NH_4)_6[P_2W_{18}O_{62}]$ for HUVEC cells. Points, mean ± SD (**n** = 5 per group). The %inhibition was calculated using the following equation: %inhibition = 100 - $[A_{(bFGF+POM)} - A_{control}] / [A_{bFGF} - A_{control}] \times 100$, where A = OD_{570}. Mean %inhibition was then calculated based on the **n** carried out.

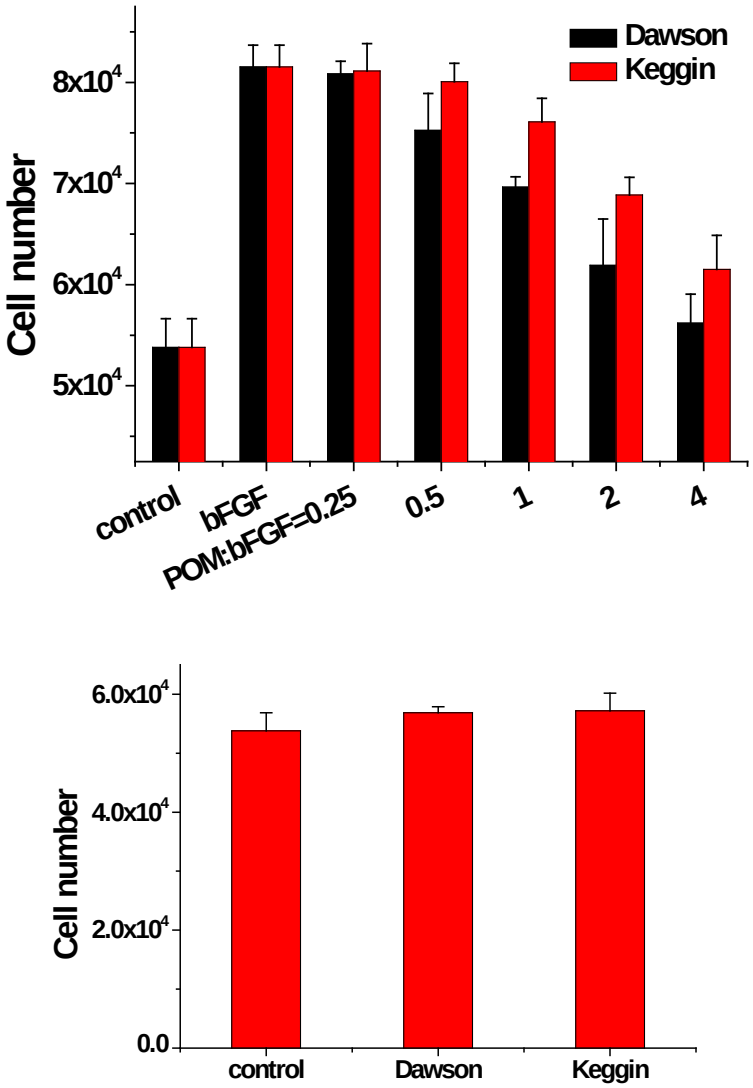

Figure S18. Inhibition of DNA synthesis by POMs. HUVEC were plated into 48-well plates and were grown to subconfluency. After serum starvation for 24 h, cells were incubated with bFGF in the presence of increasing doses of POMs for further 48 h. Analysis of DNA content was carried out by propidium iodide staining and assessing the amount of bound dye using flow cytometry. (Int. J. Exp. Path. 2009, 90, 195).